

# Dissolution Behavior of Mg from Magnesia-Chromite Refractory into Al-killed Molten Steel

著者	Chunyang Liu, Motoki Yagi, Xu Gao, Sun-Joong Kim, Fuxiang Huang, Shigeru Ueda, Shin-ya Kitamura
journal or publication title	Metallurgical and Materials Transactions B
volume	49
number	5
page range	2298-2307
year	2018-06-04
URL	<a href="http://hdl.handle.net/10097/00125825">http://hdl.handle.net/10097/00125825</a>

doi: 10.1007/s11663-018-1301-0

# Diffusion Behavior of Mn and Si Between Liquid Oxide Inclusions and Solid Iron-Based Alloy at 1473 K



SUN-JOONG KIM, HANAE TAGO, KYUNG-HO KIM, SHIN-YA KITAMURA,  
and HIROYUKI SHIBATA

In order to clarify the changes in the composition of oxide inclusions in steel, the effect of the metal and oxide composition on the reaction between solid Fe-based alloys and liquid multi-component oxides was investigated using the diffusion couple method at 1473 K. The measured concentration gradients of Mn and Si in the metal indicated that Mn diffused into the metal from the oxide, while the diffusion of Si occurred in the opposite direction. In addition, the MnO content in the oxide decreased with heat treatment time, while the SiO<sub>2</sub> content increased. The compositional changes in both phases indicated that the Mn content in the metal near the interface increased with heat treatment with decreasing MnO content in the oxide. Assuming local equilibrium at the interface, the calculated [Mn]<sup>2</sup>/[Si] ratio at the interface in equilibrium with the oxide increased with increases in the MnO/SiO<sub>2</sub> ratio in the oxide. The difference in the [Mn]<sup>2</sup>/[Si] ratios between the interface and the metal matrix increased, which caused the diffusion of Mn and Si between the multi-component oxide and metal. By measuring the diffusion lengths of Mn and Si in the metal, the chemical diffusion coefficients of Mn and Si were obtained to calculate the composition changes in Mn and Si in the metal. The calculated changes in Mn and Si in the metal agreed with the experimental results.

<https://doi.org/10.1007/s11663-018-1233-8>

© The Minerals, Metals & Materials Society and ASM International 2018

## I. INTRODUCTION

STEEL-WIRE-ROD products are typically used as steel cords for tire reinforcement and valve springs for intake/exhaust valve controllers. The breakage of steel wire rods during wire drawing to submillimeter sizes is caused by oxide inclusions exceeding 10 μm in diameter.<sup>[1,2]</sup> The major oxide inclusions causing the breakage of wire have been reported to be alumina (Al<sub>2</sub>O<sub>3</sub>) and spinel (MgO·Al<sub>2</sub>O<sub>3</sub>), which form during Al

deoxidation.<sup>[1,3,4]</sup> The Si-Mn deoxidizing method is useful in the manufacture of steel wire rod because small and low-melting-point oxide inclusions are produced as MnO-SiO<sub>2</sub>.<sup>[5-7]</sup> Furthermore, the oxide inclusions can also be softened by reaction with CaO-SiO<sub>2</sub>-Al<sub>2</sub>O<sub>3</sub> bearing fluxes in the secondary refining process. However, it was recently determined that the composition of softened inclusions varied upon reacting with alloying elements at hot rolling temperatures, and the composition of the oxide inclusions changed as precipitation of the solid phase increased.<sup>[8,9]</sup> In previous studies,<sup>[5-7]</sup> a given oxide, which becomes the seed for the inclusions, was added into the molten steel, and a metal sample including the small inclusions was reacted at hot rolling temperatures under the coagulation of the metal. Then, the morphology, composition, and size of the oxide inclusions were analyzed. However, their reaction mechanism has not been well studied because the size of the oxide inclusions in steel is very small. Recently, in the 304 stainless steel, the transformation rate of inclusion to change MnO-SiO<sub>2</sub> to MnO-Cr<sub>2</sub>O<sub>3</sub> was investigated by heat treatment at 1273 K to 1473 K (1000 °C to 1200 °C).<sup>[10]</sup> The Cr in the solid steel was diffused to the oxide inclusion, and the Si and Mn in the inclusion were exchanged by Cr. By simulation results using kinetic model, the transformation rate of

SUN-JOONG KIM is with the Department of Materials Science and Engineering, College of Engineering, Chosun University, 309 Pilmun-daero, Dong-gu, Gwangju 61452, Korea and also with the Institute of Multidisciplinary Research for Advanced Materials, Tohoku University, 2-1-1 Katahira, Aoba-ku, Sendai 980-8577, Japan. HANAE TAGO is with the Tohoku University, Sendai 980-8577, Japan and also with JFE Steel Corporation, 1-1, Ohgishima, Kawasaki-ku, Kawasaki 210-0868, Japan. KYUNG-HO KIM is with the Institute of Multidisciplinary Research for Advanced Materials, Tohoku University and also with Hitachi Metals, Ltd., Yasugi Works, Yasugi-cho, Yasugi, Shimane 692-8601 Japan. SHIN-YA KITAMURA and HIROYUKI SHIBATA are with the Institute of Multidisciplinary Research for Advanced Materials, Tohoku University, 2-1-1 Katahira, Aoba-ku, Sendai 980-8577, Japan.

Manuscript submitted July 11, 2017.

	Journal : <b>MMTB_11663</b> Dispatch : <b>6-3-2018</b> Pages : <b>11</b>
	MS Code : <b>1233</b> <input type="checkbox"/> LE <input type="checkbox"/> TYPESET <input type="checkbox"/> DISK <input type="checkbox"/> CP

64  $\text{MnCr}_2\text{O}_3/\text{MnSiO}_2$  in the inclusion was increased as the  
 65 increase in temperature and the decrease in the diameter  
 66 of inclusions.

67 Even if the diffusion of elements and change in  
 68 composition between the oxide inclusions and steel  
 69 occurred, the varying amounts could not be detected  
 70 and were insufficient to clarify the mechanism. There-  
 71 fore, it is difficult to clarify the reaction using real  
 72 non-metallic inclusions because they are too small to be  
 73 accurately analyzed. In this study, the effect of the oxide  
 74 composition on the diffusion behaviors of components  
 75 between multi-component oxide particles and solid at  
 76 hot rolling temperature was investigated by the diffusion  
 77 couple method. Based on the authors' knowledge, the  
 78 present study is the first to investigate the reaction  
 79 between liquid multi-component oxides and solid metal  
 80 the past several decades. The diffusion couple has  
 81 sufficient oxide present to determine the reaction and  
 82 mass transfer at the interface.

## II. EXPERIMENTS

84 The details of the experimental procedure of the  
 85 diffusion couple method were described elsewhere.<sup>[11,12]</sup>  
 86 Here, the experimental procedure is explained briefly. As  
 87 illustrated in Figure 1(a), a hole was made at the center  
 88 of the alloy (1 mm × 1 mm × 1 mm), and the crushed  
 89 oxides (2 to 3 mg) were inserted into the hole. To  
 90 prevent external oxidation of the alloy during heat  
 91 treatment, the alloy and oxide sample were enclosed in a  
 92 quartz tube with Ar gas at 20 kPa, as illustrated in  
 93 Figure 1(b). In the quartz tube, Ti foil was used to  
 94 capture the oxygen in the Ar gas. The entire enclosed

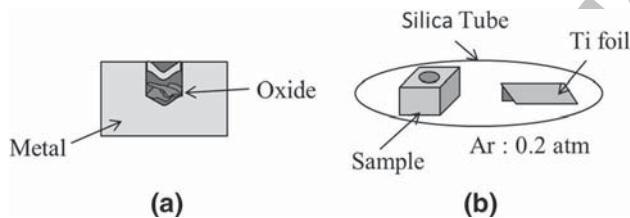


Fig. 1—Schematic image of diffusion couple samples. Figure (a) and (b) represents the images of sample of metal and oxide and preparation of sealed sample, respectively.

95 sample was heated at 1473 K (1200 °C) for 10 hours  
 96 before being quenched in water. After quenching, the  
 97 sample was removed from the quartz tube. The interface  
 98 between the alloy and oxide was examined using  
 99 electron probe microanalysis (EPMA).

100 Table I lists the initial compositions of the oxide and  
 101 metal. In runs A1, B1, and C1, the Si content in the  
 102 metal was from 1.44 to 3.34 pct by mass with a constant  
 103 Mn content. In runs C1, C2, and C3, the  $\text{CaO}/\text{SiO}_2$  ratio  
 104 in the oxide was maintained between 0.63 and 0.68,  
 105 while the MnO content was varied from 4.9 to 15.7 pct  
 106 by mass. The melting points of the oxides were analyzed  
 107 using thermo-gravimetric analysis and differential ther-  
 108 mal analysis (TG-DTA 8120, Rigaku), and the melting  
 109 temperatures of oxides 1, 2, and 3 were 1340 K, 1358 K,  
 110 and 1440 K (1067 °C, 1085 °C, and 1167 °C),  
 111 respectively.

## III. RESULTS

112 Figure 2 presents a typical image of the interface  
 113 between the oxide and the metal after the heat treatment  
 114 at 1473 K (1200 °C) for 10 hours. The oxide phase was  
 115 homogeneous, and the precipitation of oxide particles in  
 116 the metal phase near the interface was not observed. The  
 117 composition change in each phase was analyzed at a  
 118 distance of 300 μm from the interface at 5 to 50 μm  
 119 intervals. Especially, since the composition of elements  
 120 in metal side were assumed to be significantly changed,  
 121

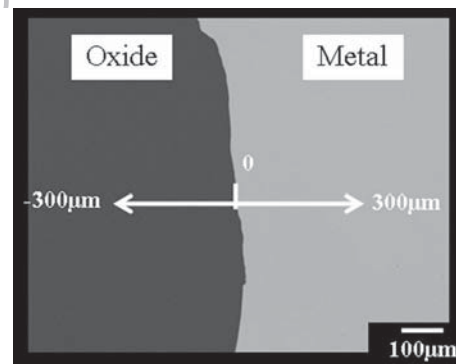


Fig. 2—Composite image of A1 after heat treatment at 1473 K for 10 h.

Table I. Initial Compositions of the Oxide and Metal

Run Nos.	Metal (Mass Pct)		Oxide (Mass Pct)							
	Si	Mn	CaO	SiO <sub>2</sub>	Al <sub>2</sub> O <sub>3</sub>	MgO	MnO	C/S		
A1	A	3.34	0.59	1	29.9	46.4	14	4.8	4.9	0.6
B1	B	2.17	0.57							
C1	C	1.44	0.53							
C2				2	27.1	43.0	13.7	5.8	10.4	0.6
C3				3	26.7	39.3	12.9	5.4	15.7	0.7

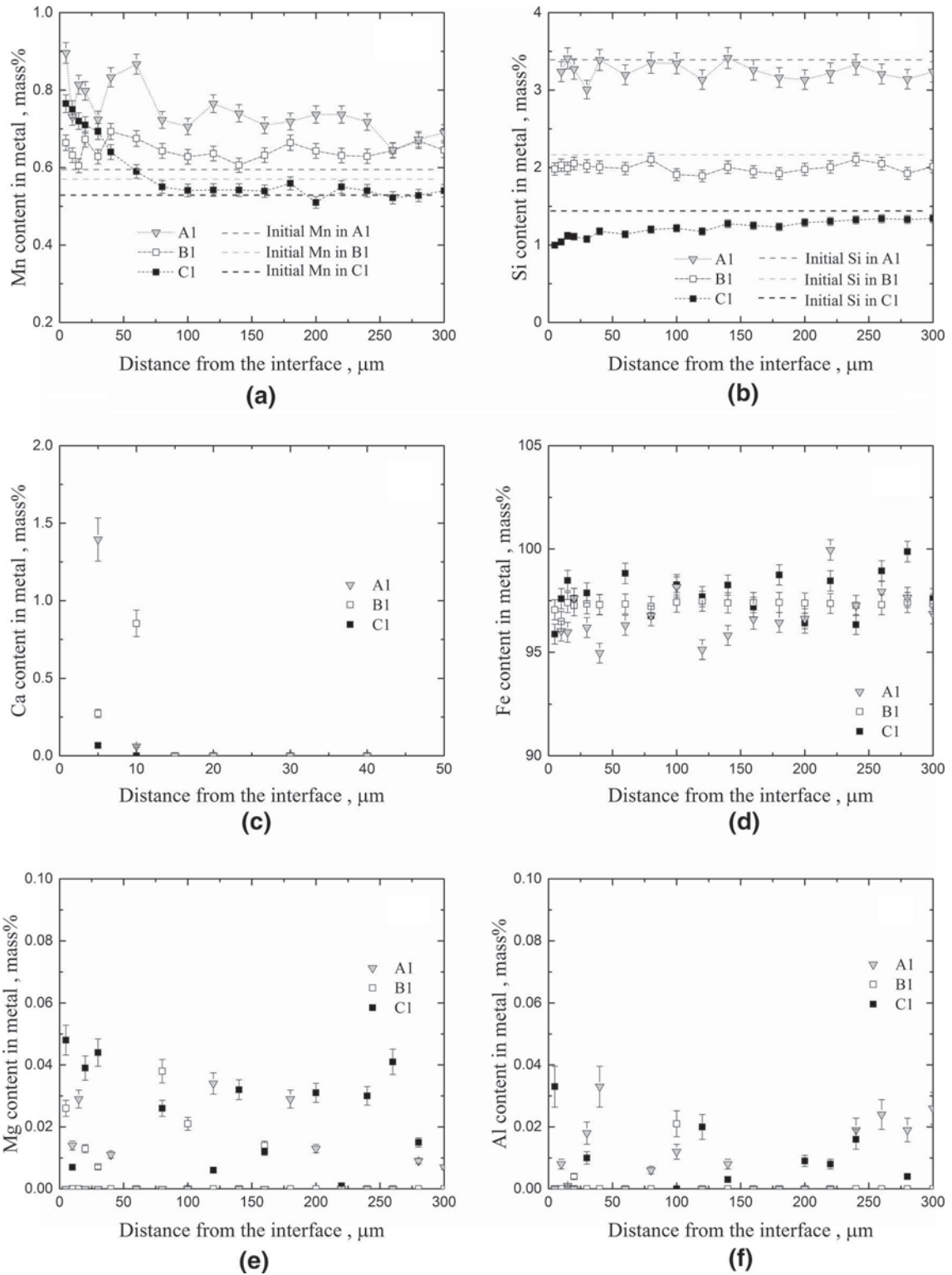


Fig. 3—Chemical composition change Mn (a), Si (b), Ca (c), Fe (d), Mg (e), and Al (f) in the metal of runs A1, B1, and C1 as a function of the distance from the interface after heat treatment at 1473 K for 10 h.

122 the 20  $\mu\text{m}$  from interface was analyzed at 5- $\mu\text{m}$   
 123 intervals.

124 Figures 3 and 4 represent the composition changes in  
 125 metal and oxide for runs A1, B1, and C1, investigating  
 126 the influence of Si content in the metal. Figures 5 and 6

represent the composition changes in the metal and 127  
 oxide for C1 through C3, investigating the influence of 128  
 MnO content in the oxide. In Figures 3, 4, 5 and 6, even 129  
 though the measured points of Mn, Si, MnO, and SiO<sub>2</sub> 130  
 were connected for the tendency of the composition 131

132 changes, those lines were not the fitting lines and had no  
 133 physical meaning. The accuracy of the measurement  
 134 results of Al, Ca, Mg, Mn, Si, and Fe were more than  
 135 95 pct, and below 0.2 pct, 0.3, 0.3, 2, 2, and 2 pct of

136 averaged error measurements, respectively. The error  
 137 bars were not shown because many points in each  
 138 figure were overlapped and difficult to determine the  
 139 precise tendency of the composition changes.

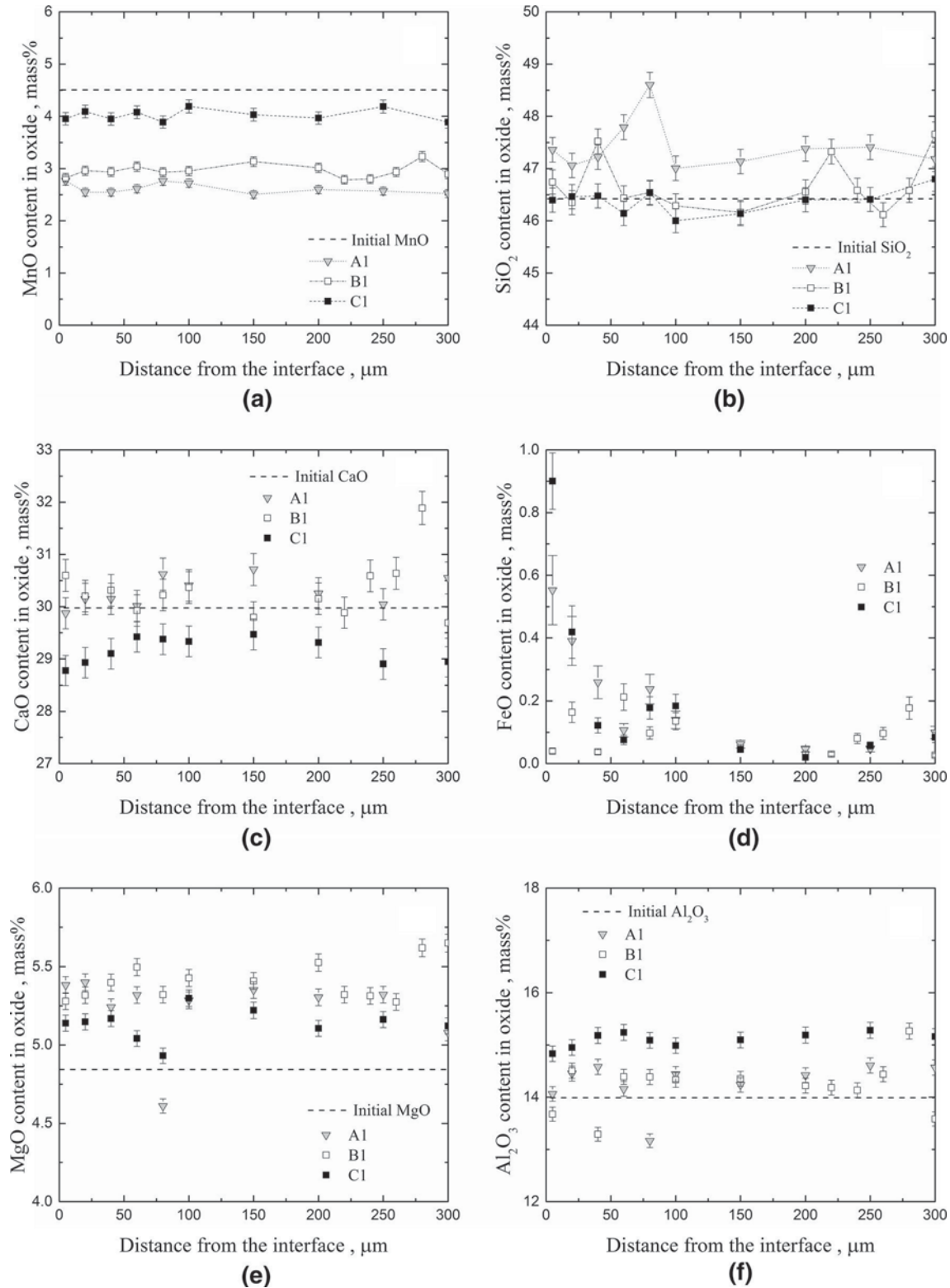


Fig. 4—Chemical composition changes in MnO (a),  $\text{SiO}_2$  (b), CaO (c), FeO (d), MgO (e), and  $\text{Al}_2\text{O}_3$  (f) in the oxide of runs A1, B1, and C1 as a function of the distance from the interface after heat treatment at 1473 K for 10 h.



140 Figure 3 shows the composition changes in Mn (a), Si  
 141 (b), Ca (c), Fe (d), Mg (e), and Al (f) in the metal of runs  
 142 A1, B1, and C1 as a function of the distance from the  
 143 interface. In Figure 3(c), the Ca contents were almost  
 144 constant more than 10  $\mu\text{m}$  from the interface. The Ca  
 145 content near the interface of A1 and B1 was close to  
 146 1 pct by mass. In the Fe-Ca binary phase diagram,<sup>[13]</sup>  
 147 the Ca solubility in  $\gamma$ -Fe was below 0.02 pct by mass at  
 148 1723 K (1450  $^{\circ}\text{C}$ ). The measured high Ca content by  
 149 EPMA analysis may be caused by the significantly small  
 150 inclusions formed during heat treatment. The Ca con-  
 151 tent in the metal was not considered because CaO in the  
 152 oxide cannot be thermodynamically reduced by either  
 153 element in the metal. The changes in Fe, Mg, and Al  
 154 were not remarkable as shown in Figures 3(d) through  
 155 (f). Although the concentrations of Fe in steel were  
 156 scattered in Figure 3(d), the averaged concentrations of  
 157 A1, B1, and C1 were, respectively, 96.4, 97.3, and  
 158 97.8 mass pct with less than 2.0 pct of measured errors.

159 By the sum of the averaged contents of Fe, and the  
 160 contents Mn and Si in Table I, the total compositions  
 161 are 100 mass pct. On the other hand, the FeO  
 162 concentrations at a distance of 5  $\mu\text{m}$  from the interface  
 163 were below 1 pct by mass and then decreased drastically  
 164 near the interface as shown in Figure 4(d). Furthermore,  
 165 the concentrations of Mg and Al in solid steel were  
 166 scattered and below 0.05 mass pct. In the present work,  
 167 the MnO in the slag can be thermodynamically reduced  
 168 by the Si in the steel. This indicates that the diffusion of  
 169 CaO, MgO, and  $\text{Al}_2\text{O}_3$  from slag to steel were unre-  
 170 remarkable as shown in Figures 4(c), (f), and (e). Each  
 171 composition in the slag was slightly changed as the MnO  
 172 decreased and as the  $\text{SiO}_2$  increased. Based on the  
 173 diffusion behaviors of Mn and Si, the diffusion length  
 174 was determined by 300  $\mu\text{m}$ , and the diffusion behavior  
 175 of Ca, Fe, Mg, and Al were not considered in this study.  
 176 In contrast, despite the similar initial concentration of  
 177 Mn, the Mn content in the metal increased in the

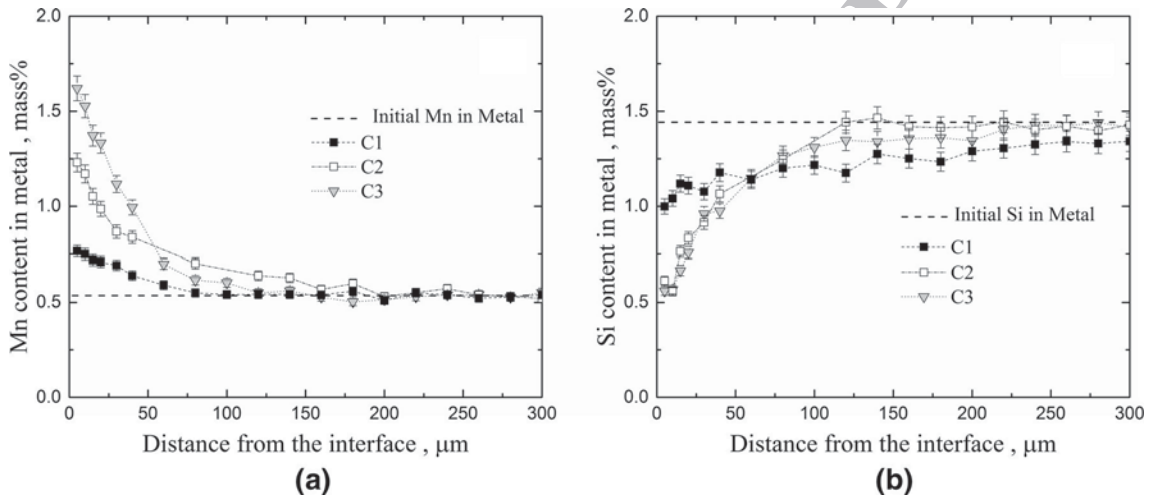


Fig. 5—Chemical composition change Mn (a) and Si (b) in the metals of runs C1, C2, and C3 as a function of the distance from the interface of the metal after heat treatment at 1473 K for 10 h.

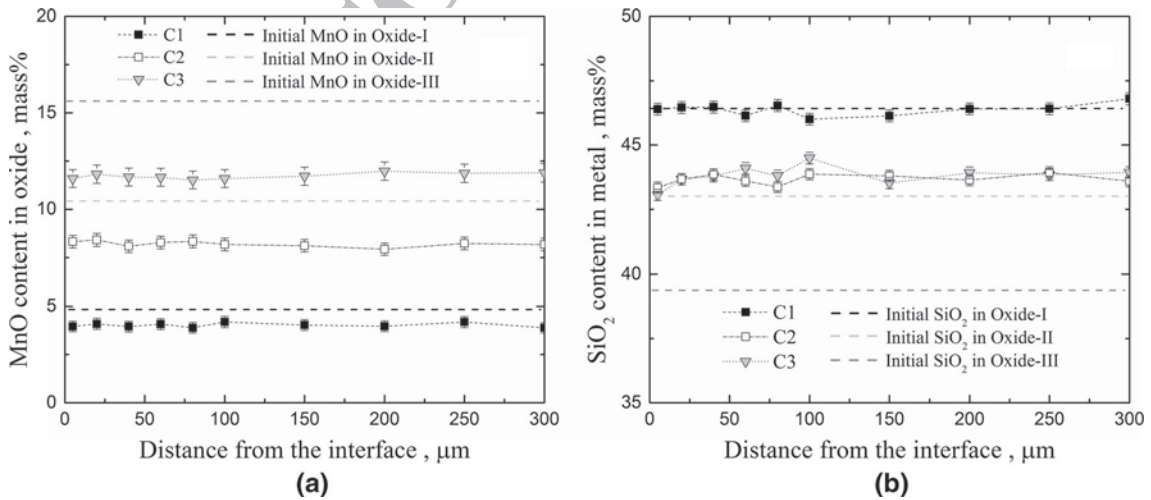


Fig. 6—Chemical composition changes in MnO (a) and  $\text{SiO}_2$  (b) in the oxides of runs C1, C2, and C3 as a function of the distance from the interface of the oxide after heat treatment at 1473 K for 10 h.

178 following order: A1, B1, and C1. As shown in Fig-  
 179 ure 3(b), the concentrations of Si in the metal decreased  
 180 after heat treatment compared to each initial composi-  
 181 tion. In particular, the changes in Mn and Si in the metal  
 182 of C1 showed the concentration gradients near the  
 183 interface of metal. When the Si content in metal was  
 184 high, such as in A1 and B1, the concentration gradients  
 185 of Mn and Si near the interface were not observed, but  
 186 their concentrations were changed compared to the  
 187 initial values.

188 Figure 4 shows the composition changes in MnO (a),  
 189 SiO<sub>2</sub> (b), CaO (c), FeO (d), MgO (e), and Al<sub>2</sub>O<sub>3</sub> (f) in the  
 190 oxides of runs A1, B1, and C1 as a function of the  
 191 distance from the interface. The concentration gradients  
 192 of all the elements, except for FeO in the oxide, were  
 193 barely detectable. This finding indicated that the mass  
 194 transfer rates of all the elements in the liquid oxide were  
 195 very rapid. The FeO concentration near the interface  
 196 was not considered because its value was greatly  
 197 influenced by the Fe signal from the metal phase  
 198 because of the limited beam diameter of the EPMA.  
 199 As mentioned above, the composition changes of CaO,  
 200 MgO, and Al<sub>2</sub>O<sub>3</sub> were not remarkable compared with  
 201 the initial concentrations of these oxides. However, the  
 202 MnO content after heat treatment decreased compared  
 203 with the initial content of oxide 1. The decrease of the  
 204 MnO concentration after heat treatment was substantial  
 205 and exhibited a dependence on the increase of the Si  
 206 content in the metal of runs A1, B1, and C1. This  
 207 decrease in MnO in the oxide caused the increase in Mn  
 208 in the metal as mentioned in Figure 3(a). Furthermore,  
 209 the content of SiO<sub>2</sub> in the oxide increased slightly in the  
 210 order of A1, B1, and C1, because the Si in the metal was  
 211 diffused as shown in Figure 3(b).

212 Figure 5 shows the composition changes in Mn (a)  
 213 and Si (b) in the metal of runs C1 through C3 as a  
 214 function of the distance from the interface. Since the Fe  
 215 contents of C2 and C3 were almost constant, and the  
 216 changes in Ca, Mg, and Al of C2 and C3 were below  
 217 0.1 pct by mass as mentioned above, the diffusion  
 218 behaviors of Fe, Ca, Mg, and Al were not considered in  
 219 this study. However, the concentration gradients of Mn  
 220 and Si were observed to depend on the concentration of  
 221 MnO in the oxides. The concentration gradient and  
 222 concentrations of Mn near the interface of the metal  
 223 increased with increases in the MnO content in the  
 224 contacting oxide. In contrast, the concentrations of Si  
 225 near the interface of the metal decreased compared with  
 226 the initial Si content. Therefore, it was determined that  
 227 the Mn diffused into the metal from the oxide, while the  
 228 diffusion of Si occurred in the opposite direction. These  
 229 diffusion tendencies of Mn and Si were observed also in  
 230 the composition changes in the oxides.

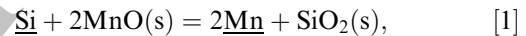
231 Figure 6 shows the composition changes in MnO (a)  
 232 and SiO<sub>2</sub> (b) in the oxide of runs C1 through C3 as a  
 233 function of the distance from the interface. Since the  
 234 mass transfer rate in the liquid oxide is larger than that  
 235 in the solid alloy, the concentration gradients in the  
 236 oxide were not observed except for FeO. In addition, the  
 237 composition changes of FeO, CaO, MgO, and Al<sub>2</sub>O<sub>3</sub>  
 238 showed similar tendency to those represented in Fig-  
 239 ure 4, and the changes in CaO, MgO, and Al<sub>2</sub>O<sub>3</sub> were

not remarkable compared to the initial concentrations. 240  
 Although similar tendencies for MnO and SiO<sub>2</sub> in oxide 241  
 were also observed, the decrease in the MnO concentra- 242  
 tion in the oxide depended on the initial concentra- 243  
 tion of the MnO before heat treatment. Furthermore, 244  
 the content of SiO<sub>2</sub> in the oxide increased under the 245  
 conditions in runs C2 and C3, as observed in Fig- 246  
 ure 6(b). For run C1, although the increase of SiO<sub>2</sub> was 247  
 not detectable, a small amount of Si diffused from the 248  
 metal, as observed in Figure 5(b). Therefore, it was 249  
 presumed that the MnO in the oxide was exchanged 250  
 with Si in the metal. 251

#### 252 IV. DISCUSSION

253 Based on the results, the diffusion of Mn and Si 253  
 between the oxide and metal was more remarkable than 254  
 that of the other elements. Figure 7 represents the 255  
 schematic image of Mn and Si diffusion between the 256  
 solid alloy and the liquid oxide. 257

258 The Mn diffused from the oxide into the metal as much 258  
 as the decrement of MnO in oxide. In contrast, the 259  
 diffusion direction of Si was the opposite from that of Mn, 260  
 and the SiO<sub>2</sub> content in oxide increased with decreasing Si 261  
 in the metal. This finding indicated that the MnO in the 262  
 oxide was reduced by the Si in the metal at the interface. 263  
 The relationship between the diffusion of Mn and Si could 264  
 be derived using the following equations: 265



$$267 \quad \Delta G_{(1)}^0 = -2272 - 36.79T \text{ J/mol.} \quad [2]$$

268 In Eq. [2], the standard free energy change at 1473 K 269  
 was calculated by extrapolating the thermodynamic 270

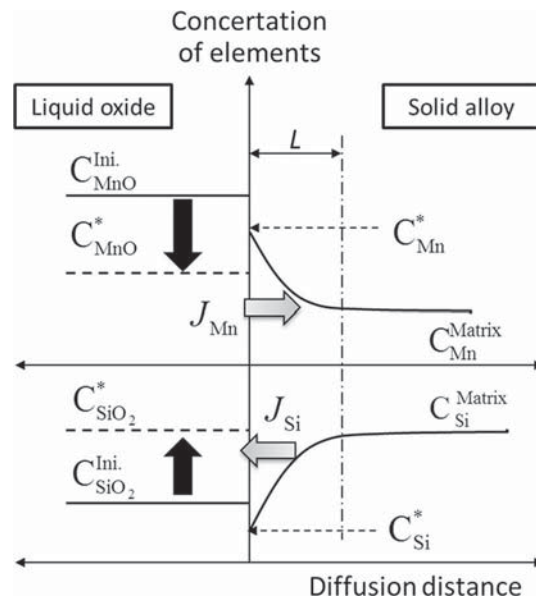


Fig. 7—Schematic image of diffusion between solid alloy and liquid oxide.

271 data.<sup>[14,15]</sup> Based on this reaction, the local equilibrium  
 272 retaliation at the interface can be derived by the fol-  
 273 lowing equation:

$$\frac{a_{Mn}^2}{a_{Si}} = K_{(1)} \frac{a_{MnO}^2}{a_{SiO_2}} = K_{(1)} \times \left( \frac{\gamma_{MnO}^2}{\gamma_{SiO_2}} \times \frac{x_{MnO}^2}{x_{SiO_2}} \right) = K_{MnSi}, \quad [3]$$

275 where  $a_i$ ,  $\gamma_i$ , and  $x_i$  are the activity, activity coefficient,  
 276 and mole fraction of component  $i$  in Eq. [1], respec-  
 277 tively. The measured values by EPMA presented in  
 278 Figures 4 and 6 were used as the mole fractions of  
 279 each oxide component in the oxide phase at the inter-  
 280 face. The  $\gamma_{MnO}$  and  $\gamma_{SiO_2}$  were derived using the regular  
 281 solution model.<sup>[16]</sup> The equilibrium constant,  $K_{(1)}$ , can  
 282 be determined using Eq. [2]. In this study, the equilib-  
 283 rium parameter of  $K_{MnSi}$  was used to express the activ-  
 284 ity ratio of Mn and Si at the interface.

285 Figure 8 presents the equilibrium ratio ( $K_{MnSi}$ )  
 286 obtained from the equilibrium relationship for runs  
 287 A1, B1, C1 through C3 as a function of the mass ratio of  
 288 (pct MnO)/(pct SiO<sub>2</sub>) in the oxide. In addition, the  
 289 ratios of [pct Mn]<sup>2</sup>/[pct Si] in the matrix of the metal  
 290 before heat treatment and the measured value at a  
 291 distance of 5 μm from the metal after heat treatment are  
 292 shown in Figure 8. As the mass ratio of (pct MnO)/  
 293 (pct SiO<sub>2</sub>) increased,  $K_{MnSi}$  increased exponentially; this  
 294 tendency was similar to that of the [pct Mn]<sup>2</sup>/[pct Si]  
 295 ratio using the analyzed values at a distance of 5 μm  
 296 from the metal side. Furthermore, the difference in  
 297 [pct Mn]<sup>2</sup>/[pct Si] at the interface and in the matrix of  
 298 the metal increased upon increasing the (pct MnO)/  
 299 (pct SiO<sub>2</sub>) ratio in the oxide. The Mn content at the  
 300 interface was considered sufficiently high to move into  
 301 the metal after heat treatment for 10 hours. Therefore,  
 302 this difference in concentrations would be related to the  
 303 driving force for the diffusion of Mn and Si between the  
 304 oxide and metal. In the cases of runs A1 and B1, when  
 305 the mass ratio of (pct MnO)/(pct SiO<sub>2</sub>) was below 0.1,  
 306 the difference in [pct Mn]<sup>2</sup>/[pct Si] before and after the  
 307 heat treatment was small, and the driving force of  
 308 diffusion was also small. Although the concentration

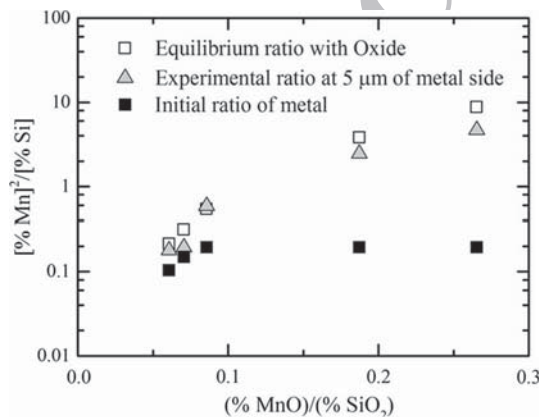


Fig. 8—Effect of MnO/SiO<sub>2</sub> ratio on the change in the equilibrium ratio ( $K_{MnSi}$ ), [pct Mn]<sup>2</sup>/[pct Si] at the interface between the metal and oxide.

gradients of Mn and Si in the vicinity of the interface on  
 the metal side were not observed for runs A1 and B1 (see  
 Figures 3(a) and (b)), the concentration changes of Mn  
 and Si in both phases occurred after heating for  
 10 hours.

Figure 9 shows the diffusion lengths of Mn and Si in  
 the metal for runs C1 through C3 as a function of the  
 differences between  $K_{MnSi}$  and the [pct Mn]<sup>2</sup>/[pct Si]  
 in the matrix before heat treatment. As illustrated in  
 Figure 9, the diffusion lengths of both elements were  
 logarithmically proportional to the differences of  $K_{MnSi}$   
 and the [pct Mn]<sup>2</sup>/[pct Si] in the matrix. In general,<sup>[16]</sup>  
 the diffusion length ( $L_M$ ) can be expressed by diffusion  
 coefficient ( $D_M$ ) of Mn or Si, and the heating time ( $t$ )  
 using the following equation:

$$\left( \frac{L_M}{2} \right)^2 = D_M t. \quad [4]$$

In this equation, when the heating time is constant,  
 the changes in diffusion length depend on the diffusion  
 coefficient. This means that the diffusion coefficients  
 for Mn and Si in the present work were dependent on  
 the driving force as well as the difference in [pct Mn]<sup>2</sup>/  
 [pct Si] between the interface and matrix. Furthermore,  
 the diffusion length of Si was larger than that of Mn  
 despite the same heating time. This result was caused  
 by the larger diffusion coefficient of Si in solid Fe com-  
 pared with that of Mn. Therefore, the diffusion of Mn  
 in the metal was assumed to be the rate-limiting step  
 in this system because the mass transfer in the liquid  
 oxide was more rapid than that in the solid metal.

In order to clarify the relationship between the driving  
 force by the thermodynamic parameter and the diffusion  
 of Mn and Si, the diffusion coefficients of Mn and Si are  
 necessary to be considered by the concentration differ-  
 ence between the interface and matrix. In Figure 7, the  
 diffusive fluxes of Mn and Si are represented by  
 classifying the liquid oxide and the solid metal based  
 on different diffusion rates. The chemical diffusion  
 coefficients of Mn and Si in the metal were obtained in  
 the present study. As shown in Figure 7, the diffusive  
 fluxes of Mn and Si,  $J_{Mn}$  and  $J_{Si}$ , should be in balance

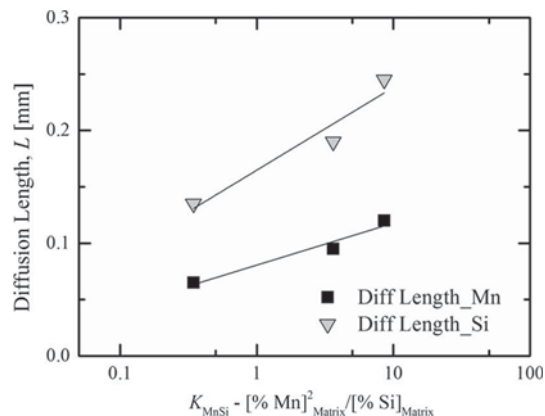


Fig. 9—Comparison of diffusion lengths of Mn and Si for C1, C2, and C3 as a function of the difference in [pct Mn]<sup>2</sup>/[pct Si] between the interface and matrix.



349 between the oxide and the alloy, and the flux of element  
350 M in the solid alloy is represented by Fick's second law:

$$\frac{\partial C_M}{\partial t} = \frac{\partial J_M}{\partial y} = D_{MnSi} \frac{\partial^2 C_M}{\partial y^2}, \quad [5]$$

352 where M is Mn and Si, and  $C$ ,  $J$ ,  $t$ , and  $y$  are the con-  
353 centration, the diffusive flux, the time, and the diffusive  
354 distance, respectively.  $D_{MnSi}$  is the inter-diffusion coef-  
355 ficient between the diffusive fluxes of Si and Mn. On

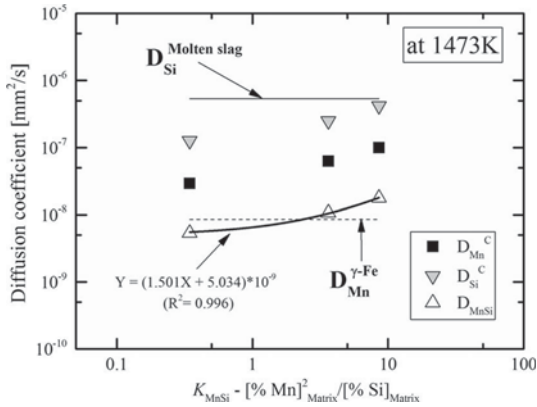


Fig. 10—Comparison of chemical diffusion coefficients of Mn and Si with the self-diffusion coefficient as a function of the difference in  $[\text{pct Mn}]^2/[\text{pct Si}]$  between the interface and matrix.

the basis of Darken's equation,<sup>[18]</sup> this coefficient can  
be represented by thermodynamic parameter as

$$D_{MnSi} = (D_{Mn \cdot X_{Si}} + D_{Si \cdot X_{Mn}}) = kT(B_{Mn \cdot X_{Si}} + B_{Si \cdot X_{Mn}}) \left( 1 + \frac{d \ln \gamma_{Mn}}{d \ln X_{Mn}} \right), \quad [6]$$

where  $k$ ,  $T$ , and  $B_M$  are the Boltzmann's constant,  
temperature, and the atom mobility of M element,  
respectively. From Eq. [6], the relationship between the  
chemical diffusion coefficient and the ideal diffusion  
coefficient can be obtained as

$$D_M = kTB_M \left( 1 + \frac{d \ln \gamma_M}{d \ln X_M} \right) = kTB_M \left( \frac{d \ln a_M}{d \ln X_M} \right). \quad [7]$$

When the self-diffusivity of a given element was investigated by the movement of trace elements or isotopes, the diffusion coefficient was mainly dependent on the temperature because the activity coefficients of the elements are constants in Eq. [7]. Since the heating temperature and the heating time were constant in the present study, the diffusion behaviors of Mn and Si could not be explained by the self-diffusion coefficients. Therefore, it is necessary to obtain the diffusion coefficients of Mn and Si that vary with the driving force at the interface between the liquid oxide and solid metal. This diffusion coefficient was also called the "chemical diffusion coefficient."<sup>[18,19]</sup>

Table II. Calculation Conditions for Concentration Changes of Mn and Si in  $\gamma$ -Fe

	$D_{MnSi}$ ( $\text{mm}^2/\text{s}$ )	$[\text{Pct Mn}]^{\text{Matrix}}$	$\Delta[\text{Pct Mn}]$	$\Delta[\text{Pct Si}]^{\text{Matrix}}$	$\Delta[\text{Pct Si}]$
A1	$5.20 \times 10^{-9}$	0.75*	0.10	3.34	- 0.10
B1	$5.28 \times 10^{-9}$	0.66*	0.03	2.17	- 0.14
C1	$5.37 \times 10^{-9}$	0.53	0.30	1.40	- 0.30
C2	$1.08 \times 10^{-8}$		0.80		- 0.79
C3	$1.78 \times 10^{-8}$		1.20		- 0.84

\*\* :  $D^{\text{Self}}_{\text{Mn}}$  is  $8.52 \times 10^{-9} \text{ mm}^2/\text{s}$ .

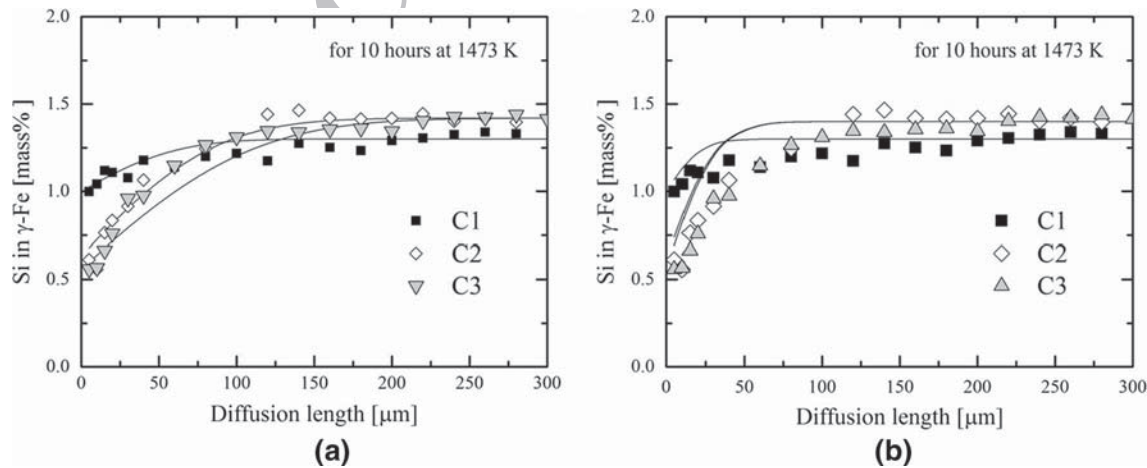


Fig. 11—Composition changes of Mn by calculation with chemical diffusion coefficients (a) and self-diffusion coefficient (b).

378 From Eq. [4], the chemical diffusion coefficient of Mn  
 379 and Si ( $D_{Mn}^C$  and  $D_{Si}^C$ ) could be obtained at 36,000 sec-  
 380 onds. Furthermore, the Mn and Si in solid  $\gamma$ -Fe were  
 381 very low, and both mole fractions in Eq. [8] were  
 382 assumed to be  $(1 - x_{Fe})$ . Therefore, from Eq. [8], the  
 383  $D_{MnSi}$  was obtained as

$$D_{MnSi} = (D_{Mn}^C x_{Si} + D_{Si}^C x_{Mn}) = (D_{Mn}^C + D_{Si}^C)(1 - x_{Fe}). \quad [8]$$

385 Figure 10 shows the comparison of the chemical diffu-  
 386 sion coefficients of Mn and Si with a self-diffusion  
 387 coefficient as a function of the difference in  $[pct Mn]^2/$   
 388  $[pct Si]$  between the interface and matrix. In this figure,  
 389 the self-diffusion coefficients of  $D_{Mn}$  in liquid oxide  
 390 and  $D_{Si}$  in  $\gamma$ -Fe were not represented as they were lar-  
 391 ger than  $\sim 10^{-5} \text{ mm}^2/\text{s}$ .<sup>[20,21]</sup> The values of  $D_{Mn}^C$ ,  $D_{Si}^C$ ,  
 392 and  $D_{MnSi}$  were increased with an increase in the dif-  
 393 ference in concentration, when the  $D_{Si}^C$  was larger than  
 394 the  $D_{Mn}^C$ . The  $D_{MnSi}$  covered a range similar to the  
 395 self-diffusion coefficient of Mn in  $\gamma$ -Fe ( $D_{Mn}^{Self}$ ). It was

determined that the rate-limiting step between the liq- 396  
 397 uid oxide and the solid alloy was governed by the dif-  
 398 fusion of Mn in the metal.

In order to compare the validity of  $D_{MnSi}$  with the 399  
 400 self-diffusion coefficient of Mn in  $\gamma$ -Fe ( $D_{Mn}^{Self}$ ), the  
 401 concentration changes in Mn and Si in  $\gamma$ -Fe were  
 402 calculated by following equations:

$$[Pct M]_t = [pct M]^{Matrix} + \Delta[pct M] \cdot \left(1 - \text{erf}\left(\frac{L}{2\sqrt{D_{MnSi}t}}\right)\right), \quad [9]$$

$$\Delta[pct M] = ([pct M]^* - [pct M]^{Matrix}), \quad [10]$$

where  $L$  is diffusion length, and  $t$  is set at 36,000 seconds. 406  
 407 The  $\Delta[pct Mn]$  is determined by Eq. [10].  
 408 Although the  $[pct M]^*$  is the concentration of M ele-  
 409 ment, it was regarded as the concentration at a dis-  
 410 tance of  $5 \mu\text{m}$  from the metal. Table II represents the  
 411 values of  $[pct M]^{Matrix}$  and  $\Delta[pct M]$  for the calculation

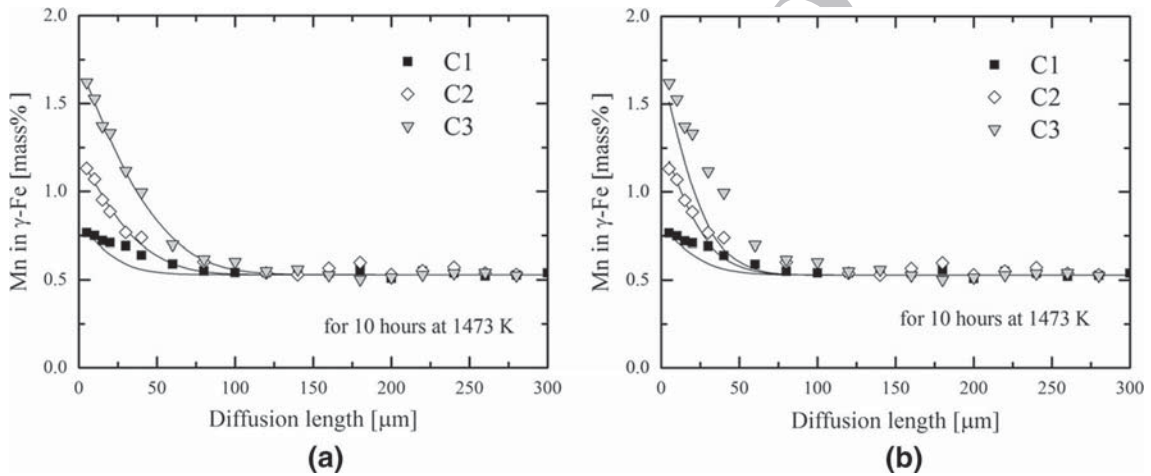


Fig. 12—Composition changes of Si by calculation with chemical diffusion coefficients (a) and self-diffusion coefficient (b).

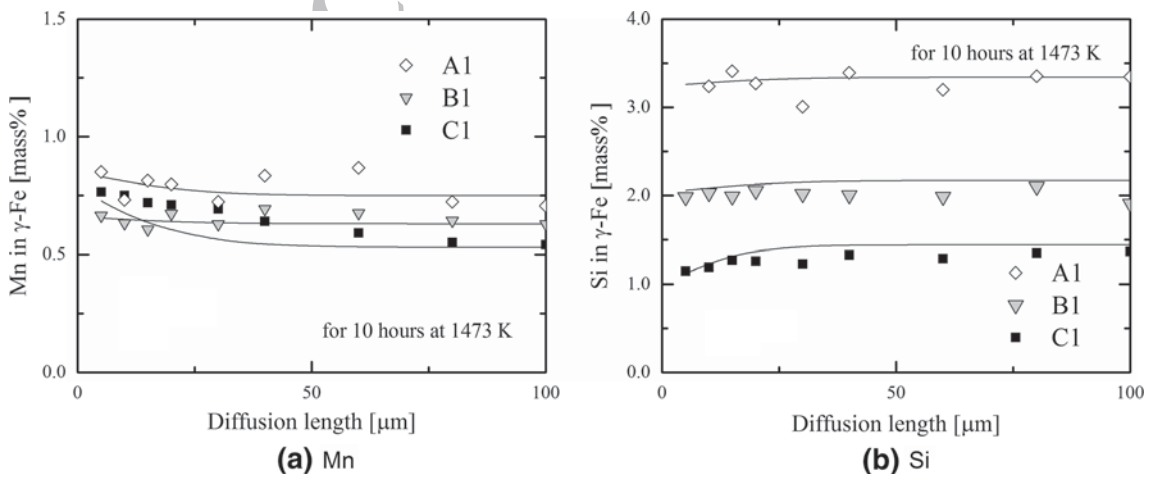


Fig. 13—Composition changes of Mn (a) and Si (b) by calculation using the  $D_{MnSi}$  of runs A1, B1, and C1 in Table II.

of concentration changes in Mn and Si in  $\gamma$ -Fe. In this table, the  $D_{\text{MnSi}}$  for each condition and the  $D_{\text{Mn}}^{\text{Self}}$  at 1473 K were also represented.

Figures 11 and 12 show the concentration changes of Mn and Si in  $\gamma$ -Fe calculated by the chemical diffusion coefficients (a) and self-diffusion coefficient (b), respectively. As shown in Figure 11(a), the calculated composition changes of Mn in  $\gamma$ -Fe showed good agreement with the experimental results compared to the calculated results of Figure 11(b). In particular, the calculation for the conditions in run C3 using the self-diffusion coefficient showed lower values compared to the experimental results of run C3, and the calculated composition gradients of C3 were close to that of C2 beyond 20  $\mu\text{m}$ . In Figure 12(a), the calculated composition changes in Si in  $\gamma$ -Fe by  $D_{\text{MnSi}}$  were in relatively good agreement with the experimental results. However, the calculated composition changes in Si in  $\gamma$ -Fe using the self-diffusion coefficient of Mn showed similar values for the conditions in runs C2 and C3.

Figure 13 shows the composition changes of Mn (a) and Si (b) by calculation using  $D_{\text{MnSi}}$  of A1, B1, and C1 in Table II. The values of  $D_{\text{MnSi}}$  for runs A1 and B1 were obtained by the relationship between the  $D_{\text{MnSi}}$  and  $K_{\text{MnSi}}$  in Figure 10. In Table II, the [pct M] $^{\text{Matrix}}$  for the conditions in runs A1 and B1 were determined from the experimental results, because the Mn content in the metal was remarkably increased by diffusion of MnO from the liquid oxide reduced by the high Si content in the metal. As shown in Figure 13, the calculated results of Mn and Si content by  $D_{\text{MnSi}}$  agreed with the experimental results. Therefore, the chemical diffusion coefficient with thermodynamic consideration at the interface was necessary to calculate the diffusions of Mn and Si between the oxide and the solid iron-based alloy.

## V. CONCLUSIONS

Based on heat treatment at 1473 K of a solid iron-based alloy and multi-component liquid oxides, the effect of the alloy and oxide compositions on the diffusion of the elements was investigated. The following conclusions were drawn:

- (A) After heat treatment, the diffusion of Mn and Si in both phases was more remarkable compared with that of the other elements (Al, Mg, Ca, and Fe). Mn diffused from the oxide into the metal, and Si diffused in the opposite direction. Although the concentration gradients of MnO and SiO<sub>2</sub> in the oxide were not detected, those of Mn and Si on the metal side with low Si content were detected. In the case of the high Si-metal, the concentration changes of Mn and Si after heat treatment were varied in the entire matrix without concentration gradients near the interface.
- (B) With increases in the initial content of MnO in the oxide and Si in the metal, the MnO content in the oxide decreased and the Mn concentration of the metal near the interface increased after heat treatment. In contrast, the Si content of the metal de-

creased, and the SiO<sub>2</sub> content in the oxide increased slightly.

- (C) The thermodynamic assessment presuming local equilibrium at the interface revealed that the [Mn]<sup>2</sup>/[Si] ratio at the interface increased upon increasing the MnO/SiO<sub>2</sub> ratio in the oxide. Therefore, the driving force for the diffusion of Mn and Si was dependent on the activities of MnO and SiO<sub>2</sub> in the oxide. The diffusion lengths of Mn and Si on the metal side were proportional to the difference of [Mn]<sup>2</sup>/[Si] between the interface and matrix. Furthermore, the chemical diffusion coefficients of Mn and Si in this study were obtained by the diffusion lengths of Mn and Si on the metal side. Using  $D_{\text{MnSi}}$  based on the obtained coefficients, the calculated changes of Mn and Si content in the metal showed good agreement with the experimental results.

These conclusions suggest the feasibility to simulate the composition change in the small oxide inclusions by using chemical diffusion coefficients between liquid oxide and solid metal. In order to simulate the mass transfer in the liquid oxide, we are currently studying the time dependency of the diffusion of Mn and Si between the liquid oxide and a Si-deoxidized alloy in greater detail.

## ACKNOWLEDGMENTS


The ISIJ Research Promotion Grant of Iron and Steel Institute of Japan is acknowledged for partial financial support for this study. And this study was supported by research fund from Chosun University, 2016. We would like to appreciate Professor Katsunari Oikawa in Tohoku University for valuable comments about the diffusion coefficient and the thermodynamics.

## REFERENCES

1. T. Mimura: *182/183rd Nishiyama Kinen Kouza ISIJ*, 2004, pp. 127–50.
2. S. Okushima: *126/127th Nishiyama Kinen Kouza ISIJ*, 1988, pp. 147–66.
3. A. Yoshimochi, K. Yokoe, T. Shibata, and Y. Oki: *Wire J. Int.*, 1983, vol. 16, pp. 224–26, 228, 231.
4. E. Stmpa and M. Cipparrone: *Wire J. Int.*, 1987, vol. 20, pp. 44–55.
5. H. Iwai, B. Tsujino, S. Isa, and T. Ao: *Tetsu-to-Hagane*, 1968, vol. 54, pp. 1037–46.
6. H. Iwai, B. Tsujino, S. Isa, and T. Ao: *Tetsu-to-Hagane*, 1969, vol. 55, pp. 887–900.
7. K. Takano, R. Nakao, S. Fukumoto, T. Tsuchiyama, and S. Takaki: *Tetsu-to-Hagane*, 2003, vol. 89, pp. 616–22.
8. W. Choi, H. Matsuura, and F. Tsukihashi: *ISIJ Int.*, 2011, vol. 51, pp. 1951–56.
9. H. Shibata, K. Kimura, T. Tanaka, and S. Kitamura: *ISIJ Int.*, 2011, vol. 51, pp. 1944–50.
10. Y. Ren, L. Zhang, and PC Pistorius: *Metall. Mater. Trans. B*, 2017, vol. 48B, pp. 2281–92.
11. K-H Kim, S-J Kim, H. Shibata, and S. Kitamura: *ISIJ Int.*, 2014, vol. 54, pp. 2144–53.
12. K-H Kim, H. Shibata, and S. Kitamura: *ISIJ Int.*, 2014, vol. 54, pp. 2678–86.

- 529 13. H Okamoto: *J. Phase Equilib. Diffus.*, 2010, vol. 31, pp. 88–  
530 90. 537  
531 14. O Knacke, O Kubaschewski, and K Hesselmann: *Thermochemical*  
532 *Properties of Inorganic Substances*, 2nd ed., Springer, Verlag  
533 Stahleisen, Dusseldorf, 1991. 538  
534 15. ET Turkdogan: *Physical Chemistry of High Temperature Tech-*  
535 *nology*, Academic, New York, 1980, p. 81. 539  
536 16. S Banya: *ISIJ Int.*, 1993, vol. 33, pp. 2–11. 540  
17. PG Shewmon: *Diffusion in Solids*, McGraw-Hill, New York, 1963, 541  
p. 8. 542  
18. LS Darken: *Trans. AIME*, 1948, vol. 175, p. 184. 543  
19. L Boltzmann: *Ann. Phys.*, 1984, vol. 53, pp. 959–64. 544  
20. Tekko-Binran, *Handbook of Iron and Steel*, 3rd ed., ISIJ, Mar-  
uzen, Tokyo, 1981, pp. 350.  
21. K Nagata, N Sata, and K Goto: *Tetsu-to-Hagane*, 1982, vol. 68,  
pp. 1694–1705.

UNCORRECTED PROOF

	Journal : <b>MMTB_11663</b> Dispatch : <b>6-3-2018</b> Pages : <b>11</b>
	MS Code : <b>1233</b> <input type="checkbox"/> LE <input type="checkbox"/> TYPESET <input type="checkbox"/> CP <input type="checkbox"/> DISK